SHS PERFORMANCE FOR DIFFERENT FLUX LEVELS

TABLE OF CONTENTS

1 Applicable and reference documents

1.1 Applicable documents

AD1 VLT-TRE-ESO-14690-4724 Issue 1, SHS and PWS comparison report.

AD2 VLT_TRE_SPH-14690-0248 Issue1, SPHERE AO analysis report.

2 SHS optimization

As explain in the *"SHS and PWS comparison test report"* (AD1) the SHS wave front sensor was under the foreseen performance. The wave front sensor was optimized to achieve the expected performance and the experiments were repeated only for the SHS improving the experimental setup.

On this report, the main modifications are summarized and the new results are shown.

2.1 RTC

The RTC computer was improved adding a second CPU. This improves the stability of the RTC, since the computing power required by the MATLAB RTC is high. In addition the speed of the RTC is controlled by the frame acquisition of the CCD camera. The CCD camera is set at a speed lower than the maximum capability of the RTC. Thus, the RTC hast to wait always a new frame. On this way it is controlled the possible loss of frames and assure a constant loop speed.

2.2 IM acquisition optimization

The IM acquisition, at present, takes around 40 minutes. The method consists on measure the zonal Haddamard matrix for a set of cycles. In each cycle 1024 Haddamard patterns are sent and measured. Each pattern was measured 10 times on the up position and 10 times on the down position in order to subtracts the static component. This measurement was optimized using the push -pull method, we measured the up position and just after the down position (10 times each up-down). On this way the atmosphere is frozen and a possible contribution avoid.

To optimized the speed of this measurement we need to know the interval time between a command is applied and the first frame where is recorded the full actuators signal on the sensor. Thus, for a certain frame speed we could know which is the minimum number of frames to skip to obtain the first useful frame.

To find the relation frequency vs skipped frames, We acquire a continuous set of frames at a set frequency. In the middle of this sequence we send a command to the BMM and we look on the frames matrix for the first frame with the maximum signal. This matrix is acquired for different CCD frequency.

We found the optimum relation for a CCD frequency of 120 Hz and skipping 2 frames. Thus, the effective acquisition frequency is 40 Hz. The IM acquisitions takes now around 10 min for 10 iterations. Any case taking only 5 iteration (~5 min) the SNR is enough.

On this way, we controlled as well the stability loop checking the possible loss of frames.

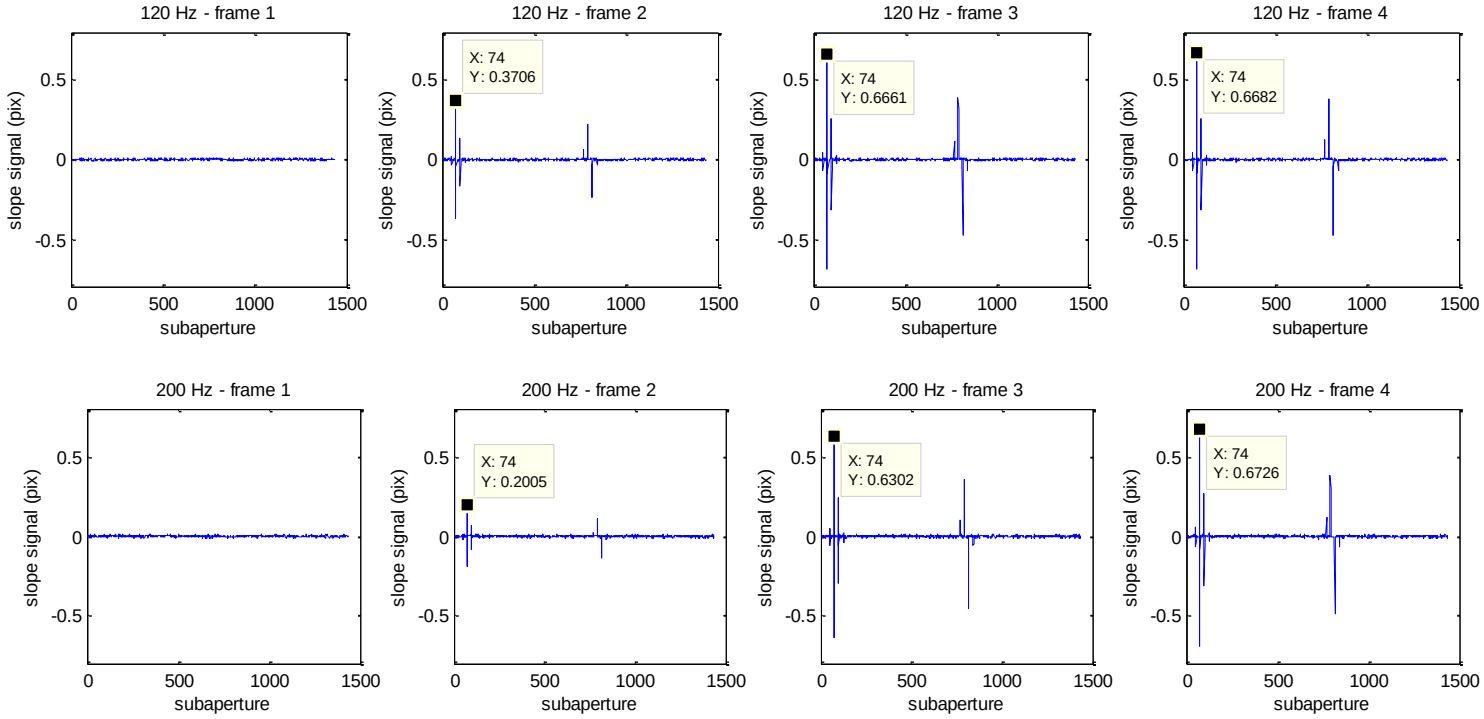

Figure 1. Example of frame acquisition for the 120 (up) and 200 Hz (down) cases. A sequence of 4 plots show the max signal produce on the detector for the 4 first frames after applying a voltage to one of the actuators (the command is applying between frame 0 and 1). For each subaperture position (on the X axe, 1-718 corresponds to X direction and 719-1436 the Y direction) we plot the signal measured on the detector (Y axe). We can track the max value obtained along the frame series that corresponds, as logical, with the same subaperture position to know the minimum number of frames to skip on IM acquisition loop.

freq (Hz)	frame 1	frame 2	frame 3	frame 4	frame 5	frame 6	Skipped	Speed
10	0.0533	0.6517	0.6779	0.6779	0.6831	0.679	2	3.33
20	0.0094	0.6096	0.6597	0.6621	0.6587	0.6596	2	6.67
40	0.0079	0.5527	0.6653	0.6666	0.664	0.6643	2	13.33
60	0.0086	0.496	0.6583	0.6578	0.6568	0.6575	2	20.00
80	0.0781	0.4535	0.6217	0.6233	0.6188	0.6244	2	26.67
100	0.0124	0.4307	0.676	0.673	0.6806	0.6746	2	33.33
120	0.0128	0.3706	0.6661	0.6682	0.6664	0.6659	2	**40.00**
150	0.0133	0.3101	0.6435	0.6737	0.6689	0.673	3	37.50
200	0.015	0.2005	0.6302	0.6726	0.6723	0.6765	3	50.00
400	0.0835	0.1135	0.6255	0.6864	0.686	0.6664	3	100.00

Table 1. Table showing the maximum slope (pix units) measured during the frame series for different CCD frequencies. The actuator command is sent between frame 0 and 1. The 7th column shows the minimum number of frames to skip on the IM acquisition loop. The last column shows the effective speed of the loop for each CCD frequency and skipping the minimum number of frames. The optimal case is found at CCD speed of 120 Hz and skipping 2 frames. The result is a loop frequency of 40 Hz.

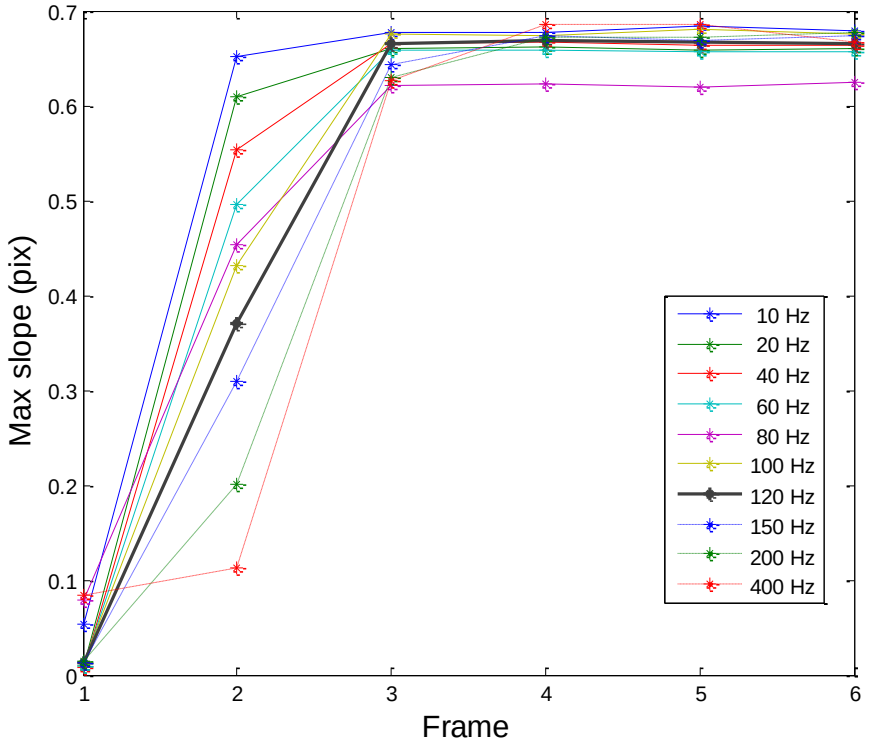

Figure 2. Plot showing the data of Table 1; maximum slope (pix units) measured during the frame series for different CCD frequencies. For frequencies down to 120 Hz it is necessary to skip two frames while for frequencies up to 150 it is necessary to skip three.

2.3 High order reconstructor

The SHS was stable using a reconstructor of 413 modes, while higher order reconstructor (600-700 modes) were not. The computing algorithm produces a modal base of 812 modes. This modal base should be truncated removing the waffle modes. These modes are expected to appear for high order modes (as shown in the Sphere report '*AO analysis report*' AD2), but, in or case appears at any position on the modal base. So a simple truncation of the last modes is not enough. We detected the waffle modes as the ones with higher stroke than expected taking into account their position on the modal base. Afterwards, this modes were verified to be waffle modes looking at the signal2mode matrix.

The final truncated modal base has 589 modes (removing also some of the last modes).

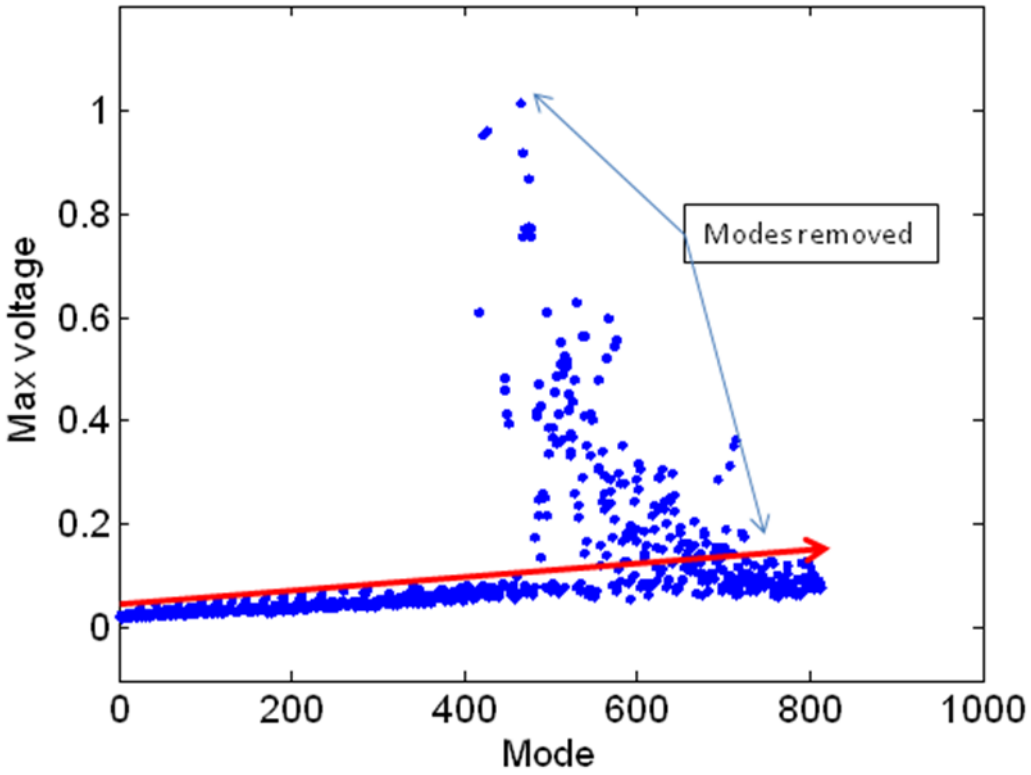

Figure 3. Max stroke required for the mode as a function of the modal order. The max voltage is computed as the max value of each column of the modal base matrix (commands x modes). The line red shows the expected tendency stroke value expected as increasing the modal order. The modes over the line are rejected.

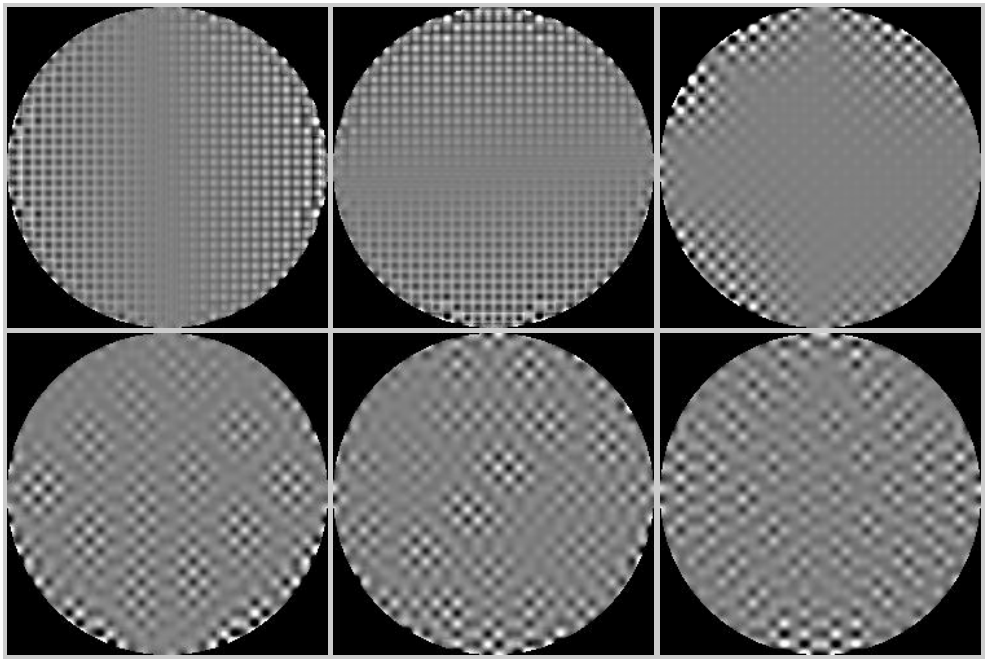

Figure 4. Example of removed waffle modes. (modes 420, 425,467 ,518, 524, 571).

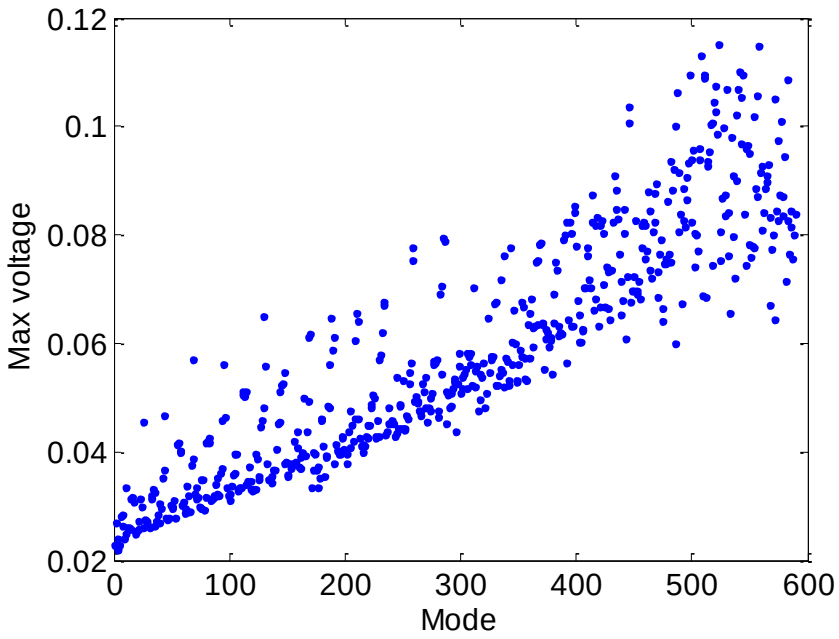

Figure 5. Max stroke required as a function of the modal order for the final truncated modal base (589 modes).

The reconstructor obtained using this new modal base is quite more stable. Any case, the performance on terms of SR was not better than the case using lower order reconstructor (~400 modes).

Two effects were observed:

- A residual waffle voltage pattern appears during the loop.
- A speckle ring on the PSF image.

The speckle rings is probably result of the waffle pattern (since it does not appear for the 412 modes case). A mean voltage pattern during the close loop operation should correspond with a static wavefront caused by static aberrations on the bench. The high frequency wavefront that would produce this voltage pattern do not correspond with any static effect and should come from an error on the wavefront reconstruction. As shown in figure 5 the waffle pattern is structured on rows. Thus we can suspect that the error could be originated by the external subapertures of the pupil since they are quite "noisy" caused by the non flatness of the BMM1 on the edges (Figure 8).

To check this hypothesis the subapertures on the edges (first and last rows) were removed from the control. It was observed that the residual voltage pattern was reduced as well as the speckle ring.

As explained on the next section, the new BMM3 is much flat than the BMM2 and will solved this problem.

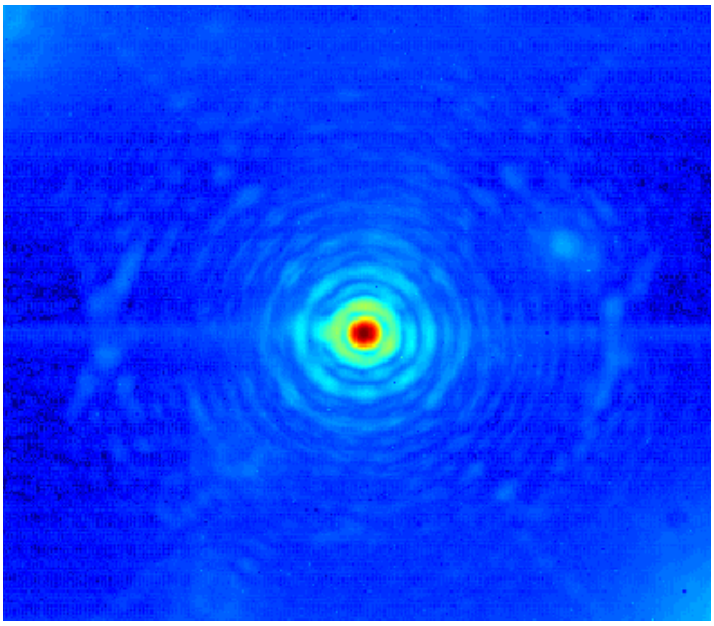

Figure 6. PSF obtained on close loop using the 589 modes reconstructor. An external ring of speckle is observed on the image.

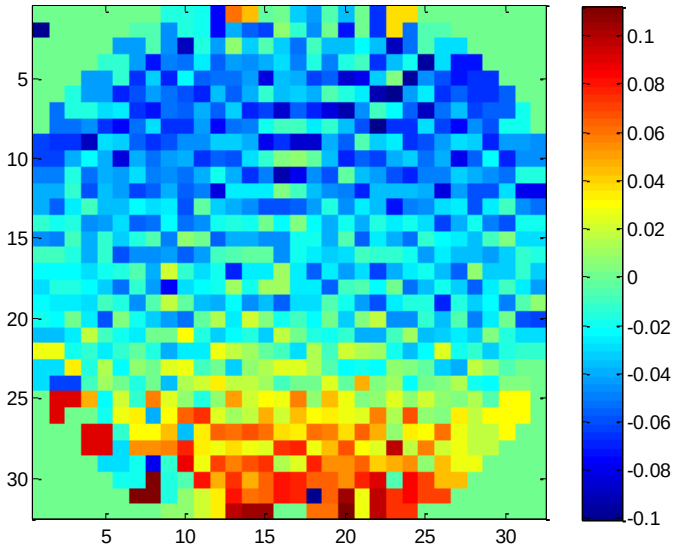

Figure 7.Mean voltage map of the BMM obtained after close loop using the 589 modes reconstructor. To remove the effect of the static aberrations on the bench we computed first the mean voltage pattern obtained on close loop using the 412 modes reconstructor and subtracting it to the ones for the 589 modes. Thus, an obvious waffle pattern is observed (Voltage scale expressed on the range [-1,1] corresponding with [0 200] volts).

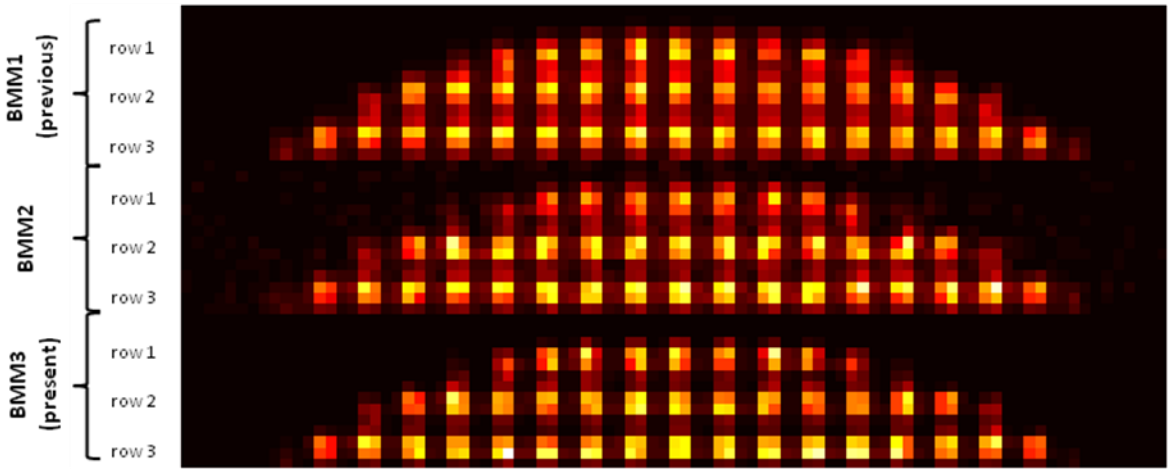

Figure 8. Image on the SHS for the three first subapertures rows (For the three BMM mirrors cases). For the BMM1 mirror the subapertures appears blurred comparing with the other two mirrors, caused by the high slope of the mirror on the edges.

2.4 The new Boston Micro-Machine mirror.

A new Boston Micro-Machine Mirror (BMM3) was bought in order to solve the ghosts problem on the IR PSF. This new mirror has a better IR coating (Ravg<1.5% @ 550-1800nm) and a stronger wedge (angle of 6 degrees between protective window and mirror). As shown in the PSF image (Figure 9) the ghost coming from the windows reflection disappeared.

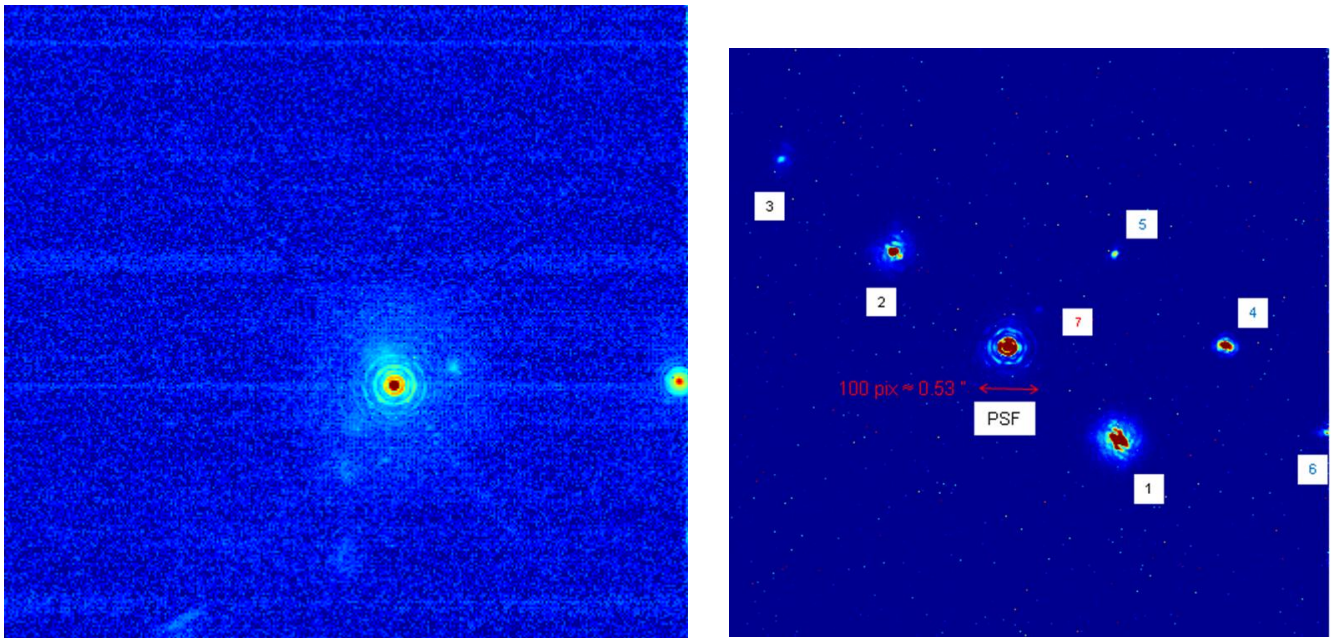

Figure 9. PSF before (right image) and after (left image) installing the new BMM3. As we can observed, ghosts 1,2,3 5 and 6 have disappeared. Ghost 4 persist since it comes from the neutral density wheel, as well as number 7 coming from the narrow filter or ITC entrance window.

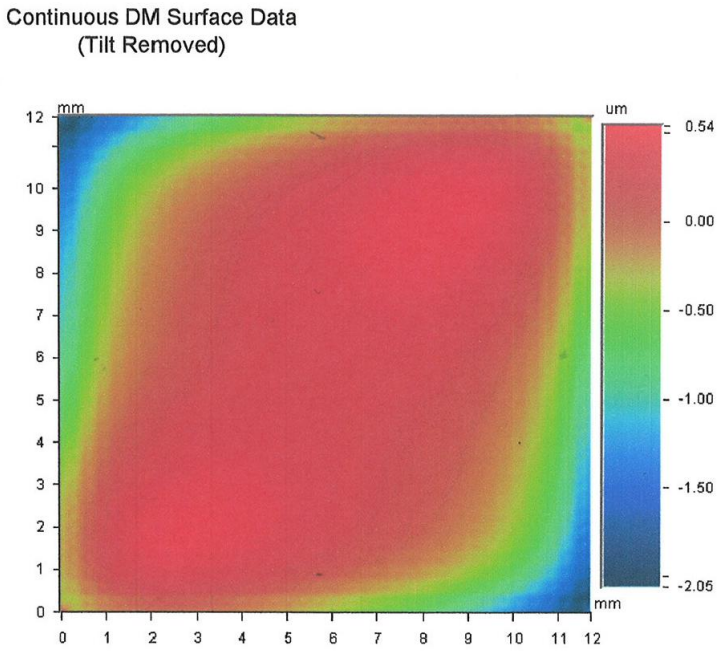

Figure 10. Surface map of the BMM3 provided by Boston Micromachine.

The surface flatness also improved comparing with the BMM1 and the blurred effect on the subapertures of the edge is fainter than before (Figure 8).

Another advantage of the new BMM is the fact that all the actuators could be controlled. Previously, two actuators were stack at zero position since they were used as pin connection for ground and TTM control. Thus, the standard VLT pupil mask were reinstalled since it is possible to use the complete pupil.

The new BMM3 was used on close loop operations using the same influence functions and same modal base that for BMM1. Thus, we assumed that the behaviour of the new BMM is similar than the previous one on term of stroke, bias, and IF shape. On the future, is foreseen to characterize the new BMM using the AOF interferometer.

The improvements on close loop operation, comparing with the previous mirror are:

- Stable close loop with 589 modes. The waffle static voltage pattern disappeared.
- Improvement of SR performance using the 589 modes respect to the 412 modes reconstructor for high flux conditions. (Section 3.3).
- The speckle ring disappeared from the PSF image. (Figure 17).

2.5 The Spatial filter problem

As explained on the SHS and PWS comparison report, the spatial filter Shack-Hartmann was not stable. We study again the performance of the SF-SHS with the BMM3. The SHS continues to be instable. As before, we could work only with the 412 modes reconstructor for periods of ~ 9 min using the 1.8 lambda/d pinhole.

We study the diverging under different situations. We discover that the SF could not work with large slope offsets. On close loop operation we need to apply offsets slopes to the SHS measurements (measured using a reference fiber on the entrance of the SHS), in

order to not take into account the differential aberrations on the SHS path. Since the slopes offsets are applied, the centroid is shift from the centre of the subapertures. It was observed that removing this offsets the loop was more stable. In addition the offsets were modified to study the effect on the loop stability. It was also observed that the subapertures were the centroid was decentred (higher offset) were the origin of the divergence of the loop.

Another experiment consists on study the effect of the stroke applied to the BMM. We measured the wavefront using the alternative source (without turbulence),so measuring only the static aberration. Afterwards, this wavefront is removed from the turbulent wavefront on close loop operations (using the standard source through the turbulence). On this way we reduced the stroke required by the DM, so, going far to the saturation regime (since the static aberrations of the bench are not corrected). It was also observed that the stability of the system increased.

The conclusion is that the instability problem using the pinhole is a combination of both large offsets that produce non linearity effects and static aberrations (i.e. stroke saturation). The HOT setup will be update with the control of the macao DM. Thus, we will be able to correct the static aberrations, so reducing the stroke required by the BMM on close loop operations. New studies will be carried under this new frame to study the performance of the SF-SHS.

2.6 Low flux condition

The comparison experiments between SHS and PWS showed a big decrease on performance (SR ~65 – 80%) for medium flux conditions (magnitude 6 and 7.5), while it would be expected for low flux condition (~ magnitude 11-12).

We want to study the effect of the L3gain on the noise level. In order to know if an increase of the gain produce a real decrease on the noise contribution. For this, we acquire a set of CCD frames without light for different gain levels (each frame with background subtraction). The standard deviation of the signal for each frame gives an idea of the noise level. Plotting the rate between gain and standard deviation for each gain shows the efficiency of the gain in the reduction of the noise. Figure 11 shows the curve for three cases: CCD shutter close (red), CCD shutter open with the same bench closure as the experiment comparison and CCD shutter open and improving the bench closure (black).

It can be observed, for the three cases, that a maximum of performance (reduction of effective noise) is reached at a gain level of ~380 (L3gain index 3100), while for higher gain the noise reduction is constant (or decrease slightly). So, it is not recommended to use higher L3 gain index than 3000 since there will not be a reduction on noise.

On the ideal case (shutter close) the minimum noise reached is 0.54 e. For this case there is not contribution of photon noise and it is only contributed by the dark and the RON. On the cases with the shutter open, the noise level is higher, contributed by the contamination of photons filtered into the bench. After improving the bench closure, the noise level decrease drastically reaching values closer to the ideal case. The photon contribution was reduced on a factor 2.3 (noise pass to 1.54 e to 0.67 e).

The photon noise contamination on the bench explain the bad results on performance for low flux conditions as it will be show on next sections.

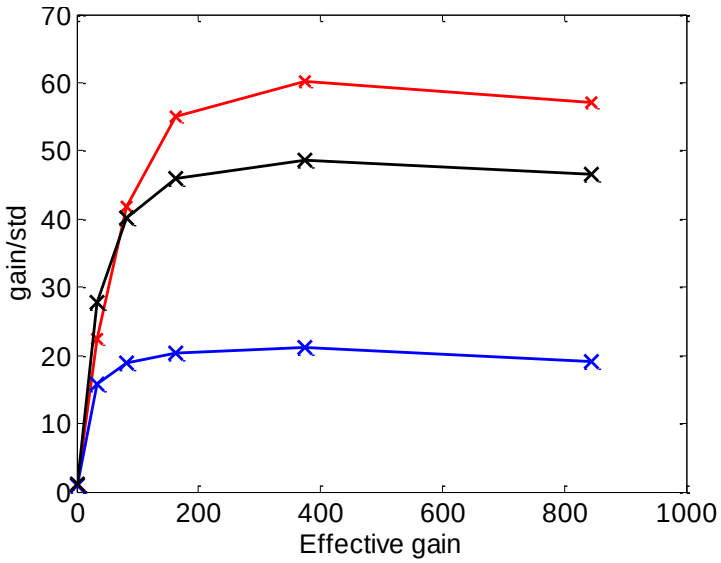

Figure 11. Plot showing the rate gain/std (noise improvement) for each gain level. The red curve show the ideal case with the shutter close while the blue and black curve show the cases with the shutter open, before and after improving the bench closure respectively .

3 Flux level study

3.1 Experimental setup

The main changes on the setup consist on the new BMM and neutral densities on the SHS setup for the flux level study. Previously we modified the flux signal on the SHS decreasing the source intensity. The problems consist on intensity fluctuations since the source lamp had to work at the minimum intensity. In addition, we were not able to reach lower flux conditions than magnitude 7.5. Another problem appears on the estimation of the flux. At low flux conditions the photon noise coming into the setup could overestimate the star magnitude.

The new approx consist on graduate neutral densities installed after the collimator on the SHS setup. On this way, computing the flux without the ND, it is possible to know with high accuracy the flux level since the ND attenuation is well know. The flux level was measured for the case without ND and maximum flux lamp (setting the lamp power supply at 12V). The flux measured was 1.37 10^9 ph/sec equivalent to 2.35 10^4 ph/sub/frame. Taking on account a loop frequency of 1.2 Khz (SPHERE case) the equivalent star magnitude is 2.1.

The ND used to study the SR vs magnitude curve were: 1.5, 2.5, 3.0 and 3.5. Table 2 show the flux variation and equivalent magnitude for the 5 experimental cases. Now it is possible to reach low flux conditions (~ 11 mag).

STAR	ND	Δ mag	magnitud
A	0	0	2.1
B	1.5	3.75	5.9
C	2.5	6.25	8.4
D	3	7.5	9.6
E	3.5	8.75	10.9

Table 2. Magnitude and ND for the 5 experimental star cases.

Since the lamp flux is set at maximum it is not necessary to readjust the ITC wheel density for each flux level (the ITC receive always the same flux), so, the static aberrations on the infrared path do not change. On other hand, it is necessary to be careful installing the ND on the SHS path in order to not introduce additional differential aberrations.

3.2 Experimental plan

The objective is to measure the performance for different flux level conditions measuring the SR and modal variance. For this we acquire the PSF image and the slopes measurements from the SHS.

For each flux case we acquire the PSF and the slopes on close loop for different gain values (0.2 – 0.4) (gain optimization). The measurements were repeated using the 589 modes and 412 modes reconstructor.

The ITC integration time (individual frames) was set at 2 seconds and the density wheel set at the position for which the signal is around 8000 counts on the ITC (the non linear range begin at 10000 counts). The images were acquired with an exposure time of 3 min 19 sec.

Table 3 show the L3gain index used for each flux level and the maximum signal reach on the CCD.

STAR	ND	L3 index	CCD max level
A	0	1200	2600
B	1.5	2600	1500
C	2.5	2900	600
D	3	2900	400
E	3.5	3000	300

Table 3. L3 gain index used and maximum signal reach on the CCD for each flux level.

3.3 Results

On this section we show the analysis for the different flux conditions. The SR is measured using the matlab routine used for NACO (more information could be found on AD1, section 8.3.3). We used a pix scale of 5.314 mas/pix and a diameter of 200 pixels (1.06 arcsec) for stars A, B and C and 240 pixel (1.28 arcsec) for stars D and E.

For each slope measurements we compute the RMS, residual variance and bandwith. These results are summarized on different tables on section 3.3.4 for each flux conditionsa nd different gains. On addition, we plot for both reconstructors the rejection transfer function (AD1 section 7.7.4) and the modal variance correction.

3.3.1 Gain optimization

To find the optimal gain there are 3 parameter to take into account SR, RMS and RV (*residual variance*; obtained by the addition of all modes coefficients variance). The RMS and RV are measured using 3000 frames, i.e., on a equivalent close loop of ~40 sec while the PSF are the result of ~ 3 minutes integration. The main parameter to take on account is the SR, but, since the SR obtained are closer it is necessary to take on account the other two parameters. So we choose the optimal gain as the one that optimized more number of these parameters.

Table 1 show the optimal gain that optimizes the different parameters and the chosen optimal gain for both reconstructors.

	589 m				412 m			
ND	SR	RMS	RV	optimal	SR	RMS	RV	optimal
0.0	0.25/0.30	0.35	0.35	**0.35**	0.30	0.40	0.40	**0.40**
1.5	0.35	0.35	0.40	**0.35**	0.25/0.30	0.35	0.35	**0.35**
2.5	0.35	0.30	0.35	**0.35**	0.25	0.30	0.30	**0.30**
3.0	0.30	0.35	0.30	**0.30**	0.25/0.30	0.25/0.30	0.30	**0.30**
3.5	0.20-0.30	0.25	0.25	**0.25**	0.20	0.25	0.25	**0.25**

Table 4. Optimal gain that optimizes the different parameters (SR, RMS, RV) on the different flux conditions and reconstructor.

Taking an eye on the modal decomposition plot for case A (ND 0 – star magnitude 2.1) we could observed that gain 0.4 seems to perform better for high order modes than 0.35, while for low order modes the maximum performance is obtained at 0.35. This suggests that a modal gain could improve the performance of the system (the reconstructor could be optimized including a gain matrix as a function of the mode order).

3.3.2 Strehl ratio and modal performance.

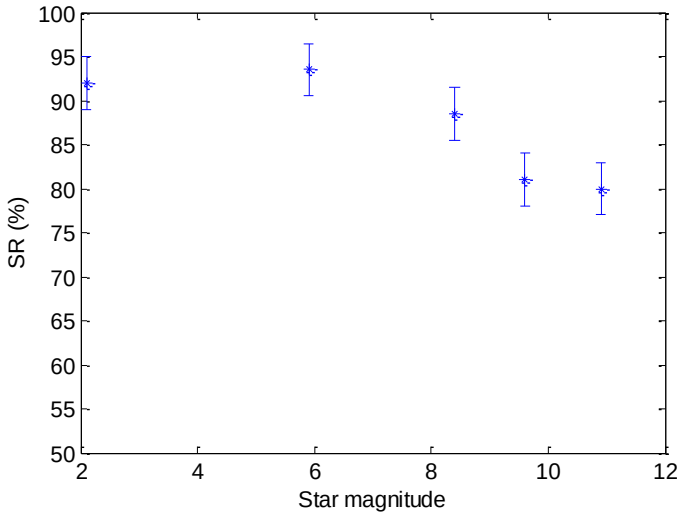

Figure 12. Best SR measurements as a function of the star magnitude. A 3% of error was assumed for the SR estimation.

ND	MAG	gain	REC	SR	RMS	RV	BW
0.0	2.1	0.35	589	92.0	0.1162	1.052	3.52
1.5	5.9	0.35	589	93.5	0.1155	1.069	3.36
2.5	8.4	0.35	589/400	88.5	0.1436	2.316	3.59
3.0	9.6	0.3	400	81.0	0.1699	3.869	2.50
3.5	10.9	0.2	400	80.0	0.2005	6.014	1.80

Table 5. Table showing the SR for the optimal gain. It shows also the RMS, RV and BW measured and the gain and reconstructor for which the SR was measured.

The measured SR for the optimal cases are shown on Figure 12. The SR values are on the range between 93.5 % and 80 %. These results are quite better than the ones exposed on the report AD1. These results also show that for medium flux levels (magnitudes 5.9 and 8.4) there is not a dramatic loss of performance. In other hand, the performance begins to decrease for low conditions (magnitudes 9.6 -10.9) as expected by simulations. As instance, for magnitude 8.5 the SR obtained on AD1 is 65 % while now is 88.5 %, which represents an improvement of ~27%.

Figure 13 shows the modal decomposition of the slope measurements on close loop for the different flux cases using the 589 modal reconstructor. As it can be observed the loop is correcting for all the 589 modes and the correction is also quite better than the results shown on AD1 for the SHS, especially after the 200 mode. The curves show that the lost of performance is similar between stars C, D and E indicating that the SR for case D could be underestimate or case C overestimate.

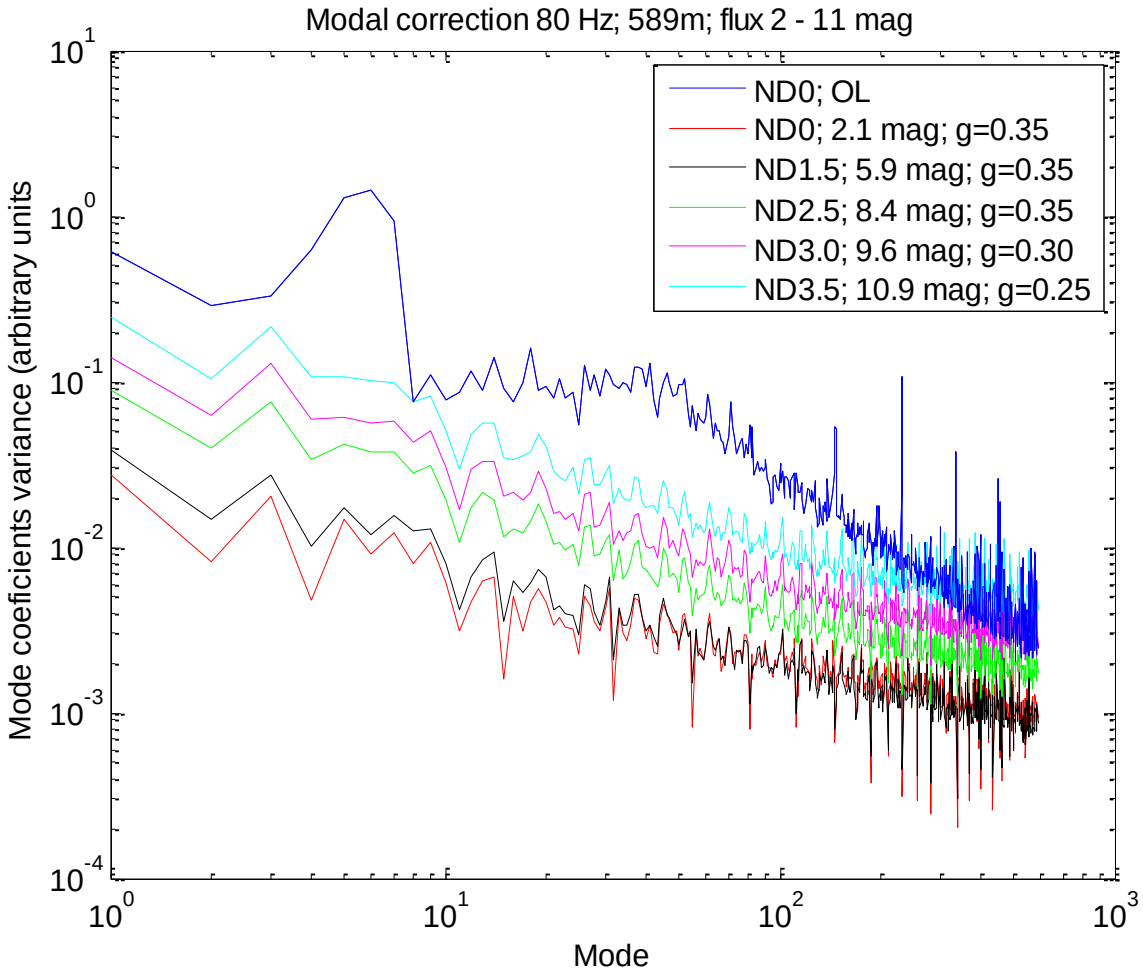

Figure 13. Modal decomposition for the 5 flux conditions using the 589 modal reconstructor.

3.3.3 PSF and contrast curves

As expected from the SR and modal decomposition results, the contrast on the halo decrease when flux decrease. Comparing these profiles with the ones showed on AD1 it is observed that the rings are quite better sharp (now rings 7-8 can be distinguished) and the profile is quite closer to the PWS profiles.

Comparing the profiles for the two reconstructor cases, it is observed how for high flux the better contrast is obtained with the 589 reconstructor, while in the low flux case is the 412 reconstructor (this is also observed from the SR and slopes rms measurments). This result suggest a modal optimization for star magnitude lower than 8.5 (Table 5).

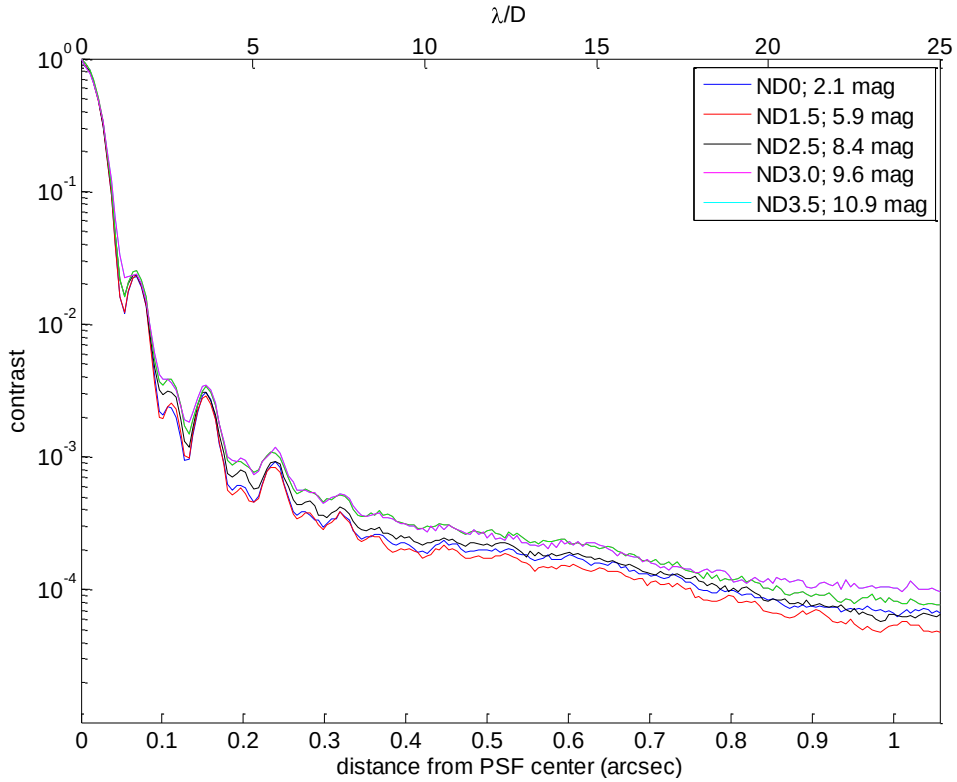

Figure 14. Contrast curves for the different flux conditions.

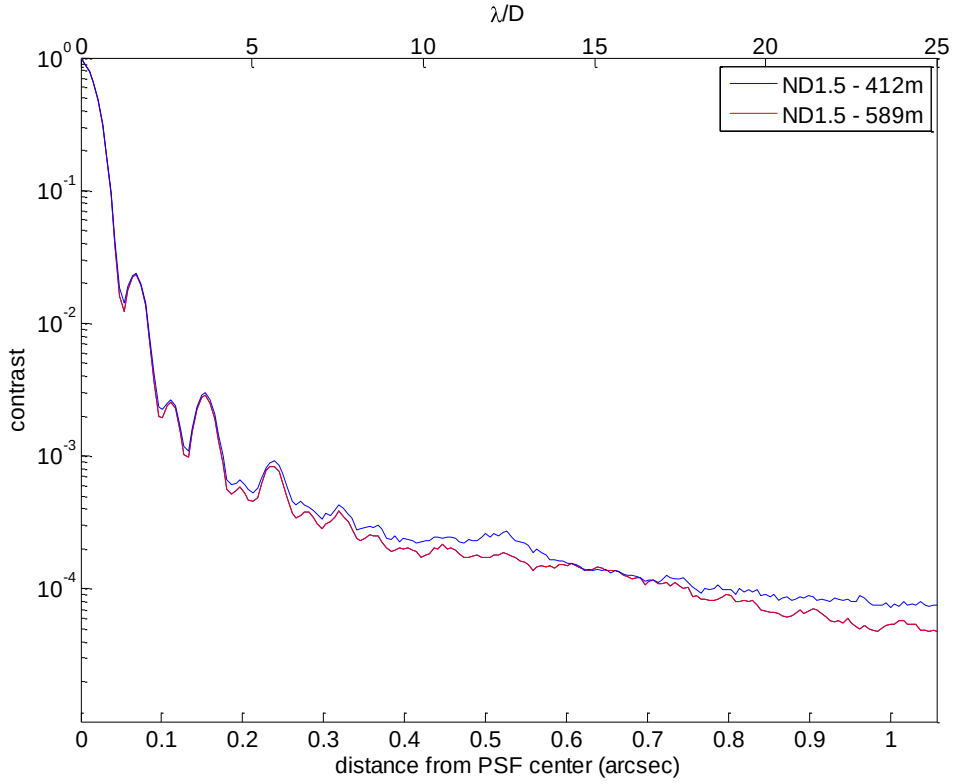

Figure 15. Contrast curves comparison between 589 and 412 modal reconstructor for high flux conditions.

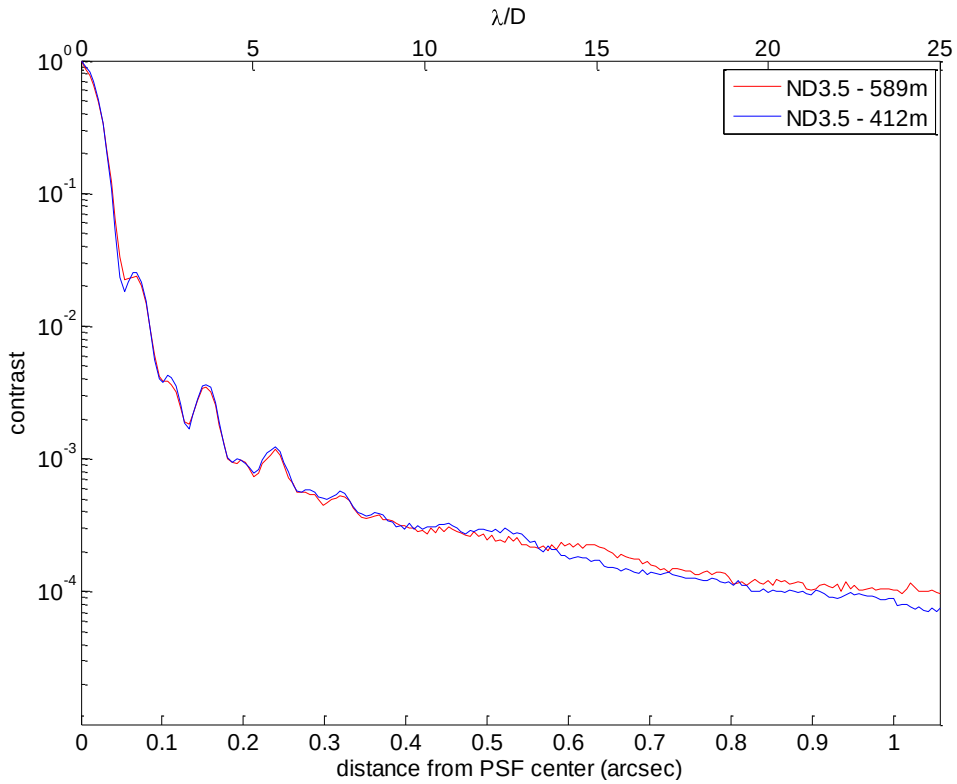

Figure 16. Contrast curves comparison between 589 and 412 modal reconstructor for low flux conditions.

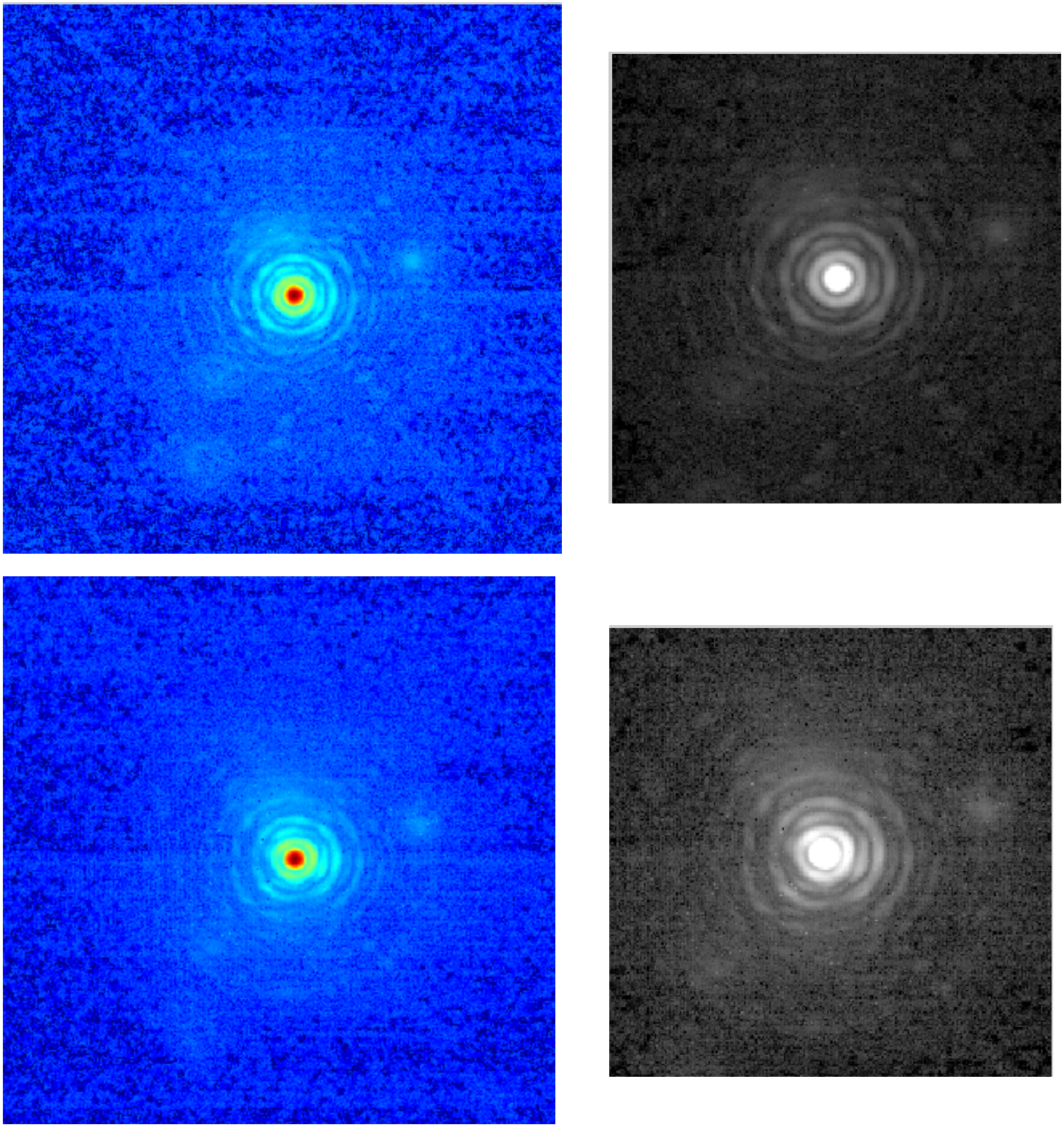

Figure 17. Best PSFs images for the star magnitude 5.9(up) and 10.9 (down) using reconstructors of 589 and 412 modes respectively. Left and right corresponds to the same image on color and B/W scale (PSF_counts^18

3.3.4 flux conditions study: plots and tables.

ND 0; MAG =2.1

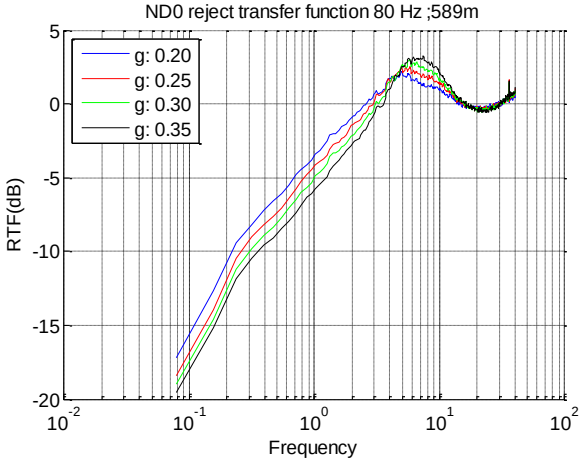

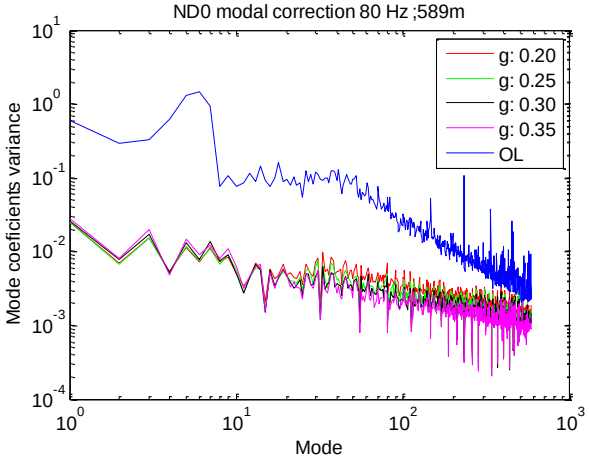

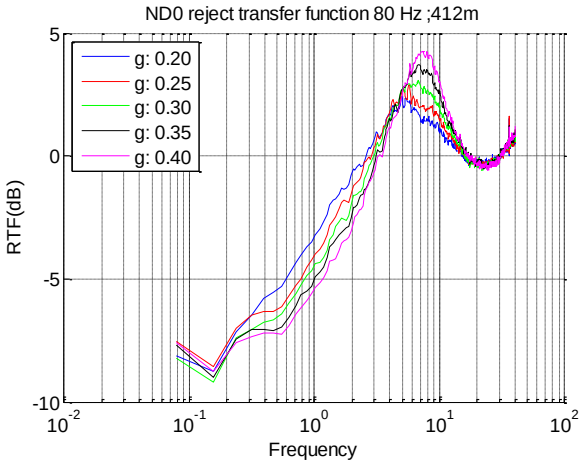

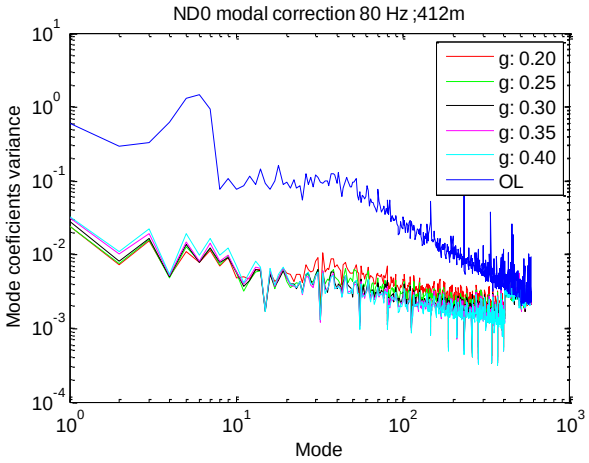

ND 0 - 589m				
gain	SR	RMS	RV	BW
0.20	0.900	0.1236	1.562	2.60
0.25	0.920	0.1204	1.308	2.89
0.30	0.910	0.1198	1.173	3.06
0.35	0.920	0.1162	1.052	3.52
ND 0 - 412m				
gain	SR	RMS	RV	BW
0.20	0.890	0.1326	1.904	2.60
0.25	0.895	0.1302	1.666	2.83
0.30	0.905	0.1277	1.536	2.97
0.35	0.900	0.1282	1.523	3.10
0.40	0.890	0.1272	1.497	3.35

ND 1.5; MAG =5.9

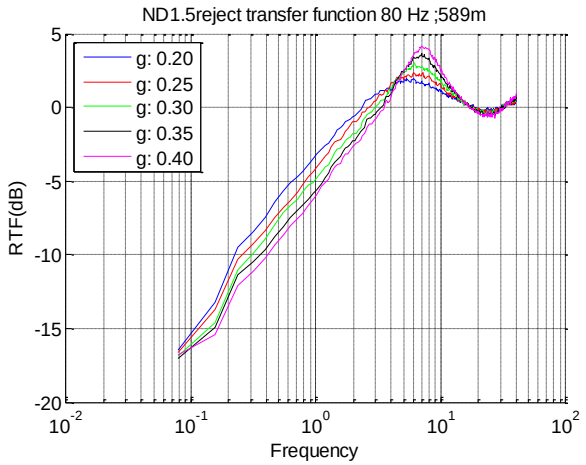

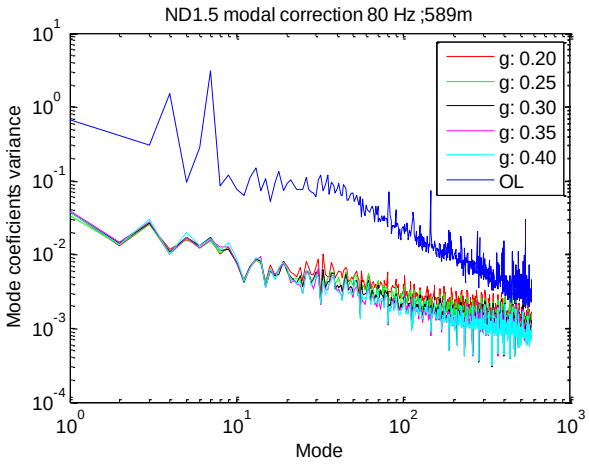

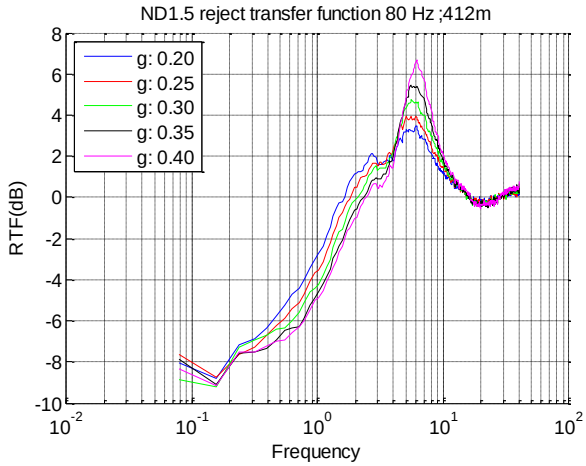

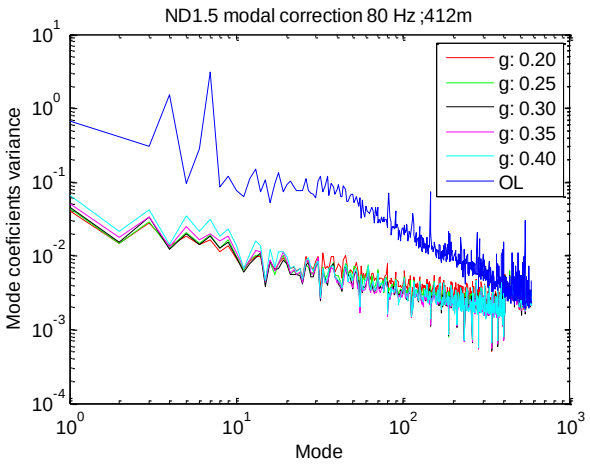

ND 1.5 - 589m				
gain	SR	RMS	RV	BW
0.20	0.900	0.1217	1.520	2.34
0.25	0.920	0.1208	1.285	2.66
0.30	0.925	0.1166	1.152	2.97
0.35	0.935	0.1155	1.069	3.36
0.40	0.930	0.116	1.043	3.67

ND 1.5 - 412m				
gain	SR	RMS	RV	BW
0.20	0.910	0.1367	2.197	2.34
0.25	0.920	0.135	2.010	2.66
0.30	0.920	0.1332	1.904	2.89
0.35	0.900	0.1326	1.905	3.59
0.40	0.880	0.1351	2.049	3.83

ND 2.5; MAG =8.4

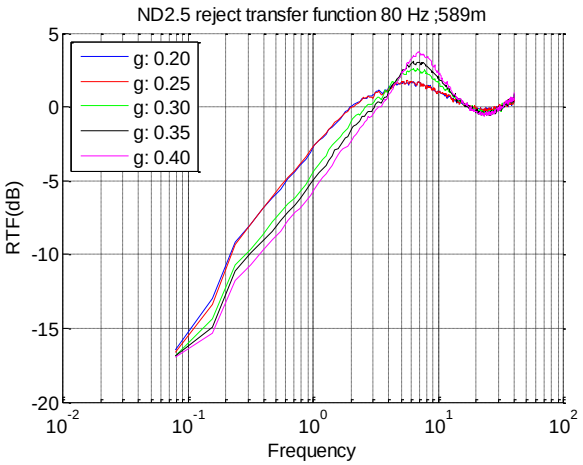

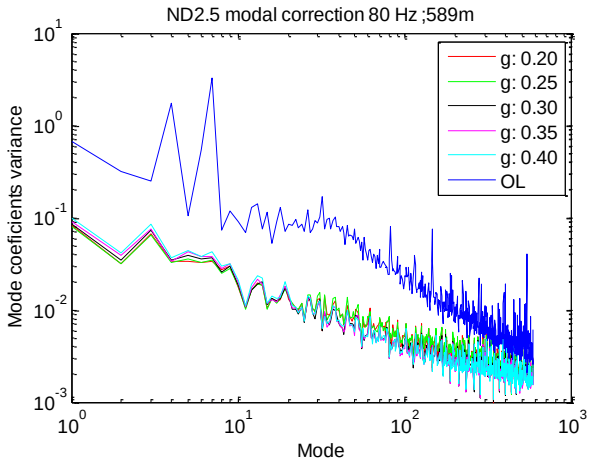

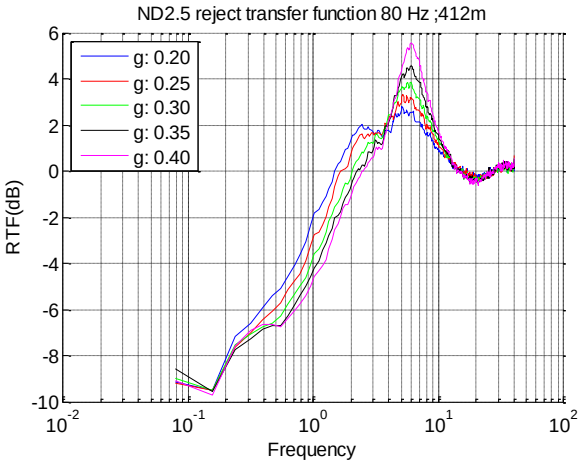

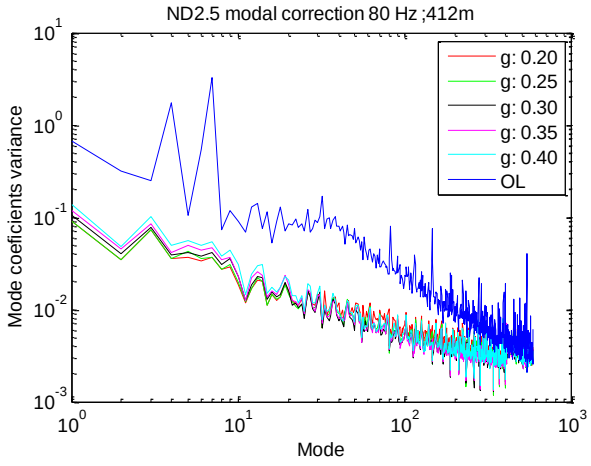

ND 2.5 - 589m				
gain	SR	RMS	RV	BW
0.20	0.880	0.1459	2.646	2.42
0.25	0.885	0.1448	2.676	2.42
0.30	0.860	0.1433	2.344	3.13
0.35	0.880	0.1436	2.316	3.59
0.40	0.870	0.145	2.365	3.83

ND 2.5 - 412m				
gain	SR	RMS	RV	BW
0.20	0.870	0.1564	3.275	1.48
0.25	0.885	0.1537	3.067	1.64
0.30	0.880	0.1513	2.975	2.03
0.35	0.870	0.1525	3.078	2.19
0.40	0.850	0.1554	3.336	2.42

ND 3.0; MAG =9.6

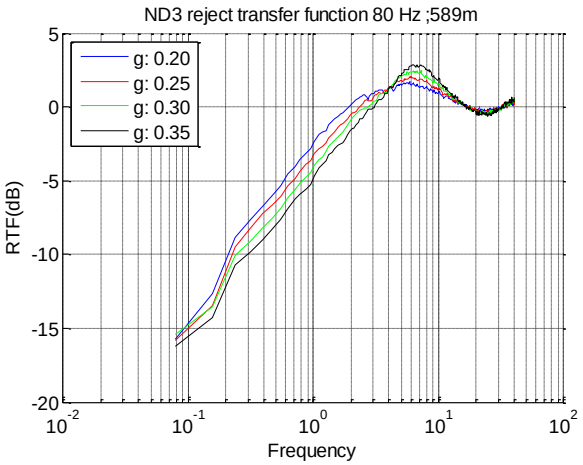

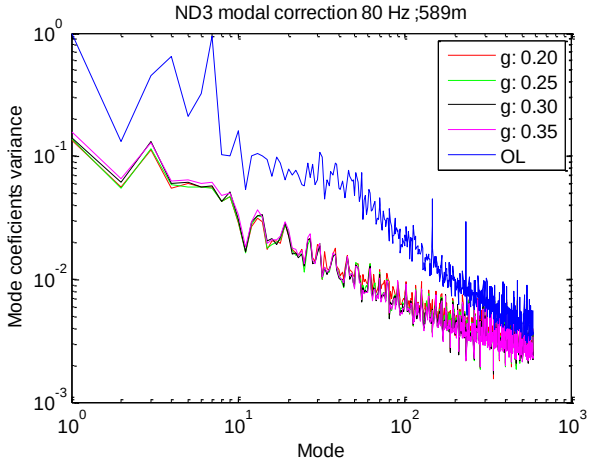

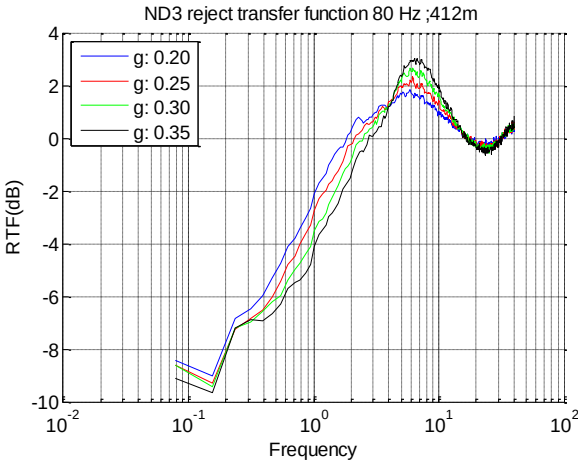

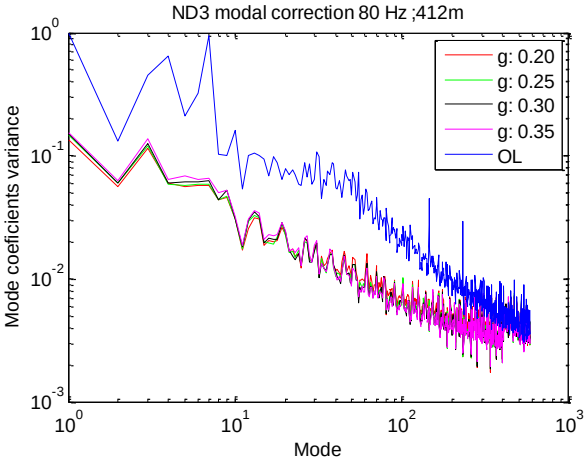

ND 3.0 - 589m				
gain	SR	RMS	RV	BW
0.20	0.790	0.1671	3.789	2.19
0.25	0.790	0.1659	3.591	2.66
0.30	0.795	0.1694	3.576	3.20
0.35	0.790	0.165	3.599	3.36

ND 3.0 - 412m				
gain	SR	RMS	RV	BW
0.20	0.805	0.1725	4.035	1.86
0.25	0.810	0.1698	3.885	2.15
0.30	0.810	0.1699	3.869	2.50
0.35	0.790	0.1685	3.903	2.77

ND 3.5; MAG =10.9

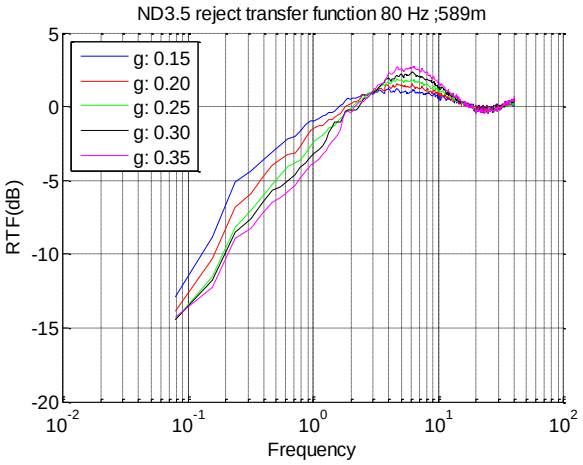

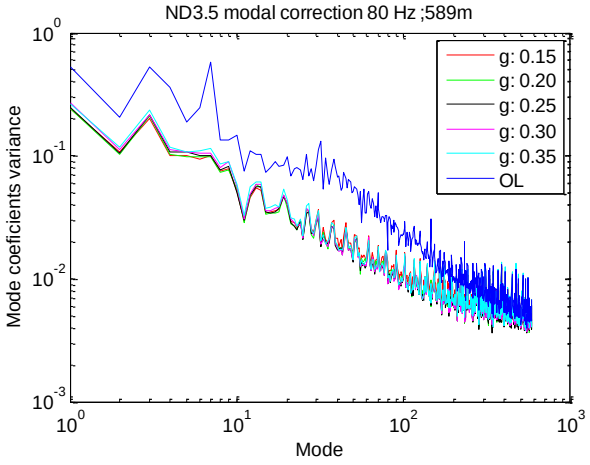

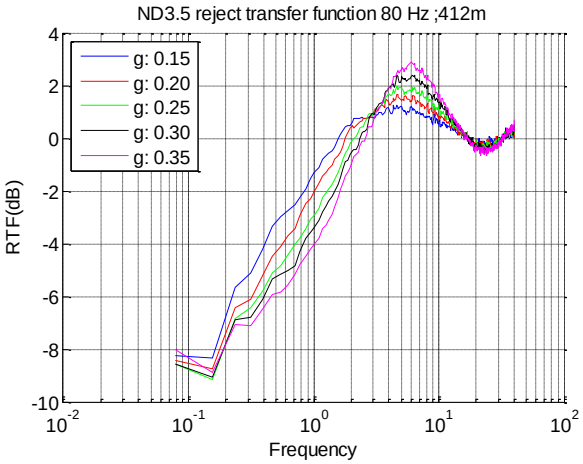

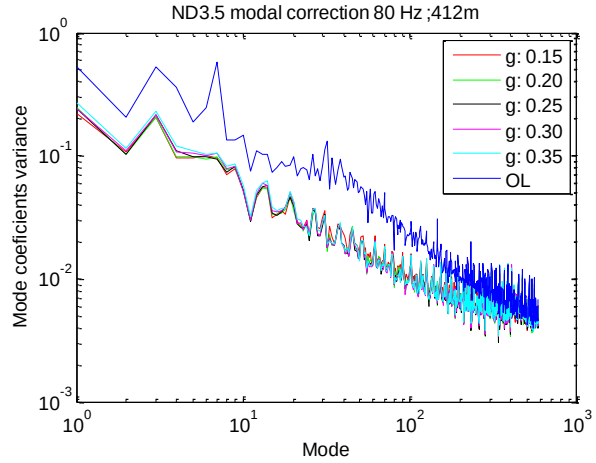

ND 3.5 - 589m				
gain	SR	RMS	RV	BW
0.15	0.785	0.2047	6.259	1.60
0.20	0.790	0.2018	5.991	1.80
0.25	0.790	0.2017	5.966	2.10
0.30	0.790	0.2048	6.131	2.19
0.35	-	0.2112	6.398	2.30

ND 3.5 - 412m				
gain	SR	RMS	RV	BW
0.15	0.780	0.2017	6.189	1.56
0.20	0.800	0.2005	6.014	1.80
0.25	0.780	0.1998	5.972	2.10
0.30	0.770	0.2011	6.079	2.34
0.35	0.765	0.2032	6.276	2.61

4 Conclusions

The new results show how the SHS is able to achieve the expected performance foreseen by simulation. This improvement on the performance is the result of improvements on the system (BMM, IM acquisition, RTC …) and the corrections of errors on the previous study (misalignments, old IM, photon contamination …).

Two of the biggest problems were resolved: high order mode reconstructor (up 400 modes) and performance at low order flux. In addition, the new BMM solve the ghost problems on the PSF. Such improvement will be extremely important on the future coronagraphic experiments.

In other hand, the biggest problem is the instability of the Spatial Filter SHS, that should increase the performance of the SHS at the PWS level. At least, the origin of the problem is well understood. The possibility of controlling the macao RTC will probably solves part of the problem.